NANO LETTERS

pubs.acs.org/NanoLett

Letter

Are There High-Density Deep States in an Atomic-Layer-Deposited Indium−Gallium−Zinc Oxide Thin Film?

Liankai Zheng, Lijuan Xing, Zhiyu Lin, Wanpeng Zhao, Yuyan Fan, Yulong Dong, Ziheng Wang, Siying Li, Xiuyan Li, Ying Wu,* Jeffrey Xu, and Mengwei Si*

Cite This: https://doi.org/10.1021/acs.nanolett.5c01673

Read Online

ACCESS | Metrics & More | Article Recommendations | Supporting Information

ABSTRACT: It has been well recognized that high-density deep states exist in indium−gallium−zinc oxide (IGZO) thin films. Many of the device characteristics of IGZO transistors, such as negative bias illumination stability (NBIS), are understood to be related to these deep states. However, in this work, it was found that the deep-state density (N_{tD}) of atomic-layer-deposited (ALD) IGZO transistors can be an ultralow value ($<2.3 \times 10^{12}/cm^3$) by the proposed NBIS-free light-assisted $I-V$ measurements so that the deep states do not affect the $I-V$ characteristics even in the subthreshold region. This work also reveals that NBIS is not related to the photoexcitation of electrons in the deep states. Our results suggest that the existence of deep states and the impact of deep states on ALD IGZO transistors may need to be revisited.

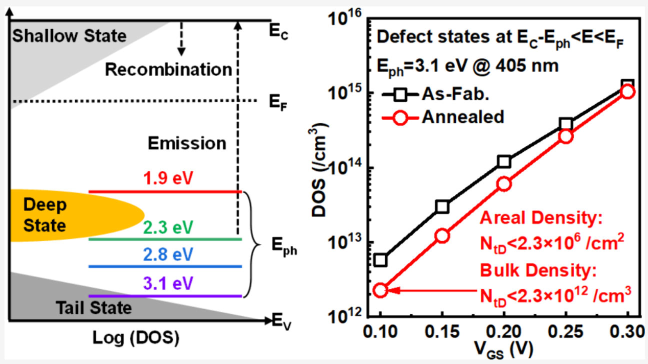

KEYWORDS: *atomic layer deposition, indium−gallium−zinc oxide, thin-film transistor, deep state*

Amorphous oxide semiconductors, such as indium−gallium-zinc oxide (IGZO), are widely used in thin-film transistors for display applications.[1−6] In particular, oxide semiconductor transistors have a very low off-state leakage current (I_{OFF}) due to the wide band gap above 3 eV, so they have also been extensively studied recently for either standalone or M3D DRAM applications.[7−17] Except for the wide band gap, the unique property of amorphous oxide semiconductors compared with single-crystalline semiconductors is the existence of subgap defect states because of the nonperiodic arrangement of atoms.[1,6] It has long been believed that there are high-density deep states located slightly above the valence band (E_V) in oxide semiconductors, as first reported through hard X-ray photoelectron spectroscopy on the order of $10^{20}/cm^3$.[18,19] The detected high-density deep states are attributed to the performance of IGZO transistors, such as negative bias illumination stability (NBIS),[20−23] positive bias stability (PBS),[22,24,25] etc., which affect the performance of IGZO transistors, especially in display applications.

However, many of the phenomena that are commonly believed to be related to deep states, such as NBIS, are concluded from indirect experiments,[20−22] but there is a lack of decisive evidence. Meanwhile, the accurate measurement of the deep-state density (N_{tD})[25−31] and the understanding of its impact on the device performance are frequently affected by the stability of the device, so the measurement and understanding of deep states in oxide semiconductors can be inaccurate and needs further clarification.

In this work, the light-assisted $I-V$ method was further developed to exclude the impact of NBIS and carrier recombination-induced underestimation. The measurement method was optimized by (1) applying only positive gate voltages to prevent the impact of NBIS during measurement and (2) using different and saturated light powers to ensure that electrons in the deep states are mostly emitted. We fabricated atomic-layer-deposited (ALD) IGZO transistors with different process conditions, and an ultralow N_{tD} of $<2.3 \times 10^{12}/cm^3$ was achieved on devices with an optimized process by the above NBIS-free light-assisted $I-V$ method. It was found that a relatively large threshold voltage shift (ΔV_{th}) caused by NBIS still exists on devices with such a low N_{tD}. The carrier density change caused by NBIS is 4 orders more than N_{tD}, suggesting that NBIS cannot be related with deep states for ALD IGZO transistors with an optimized process. Then, the mechanism of NBIS in ALD IGZO transistors was clarified to be the light-induced mobile hole generation from the valence band (E_V) to shallow states and hole trapping into the

Received: March 15, 2025
Revised: March 26, 2025
Accepted: March 27, 2025

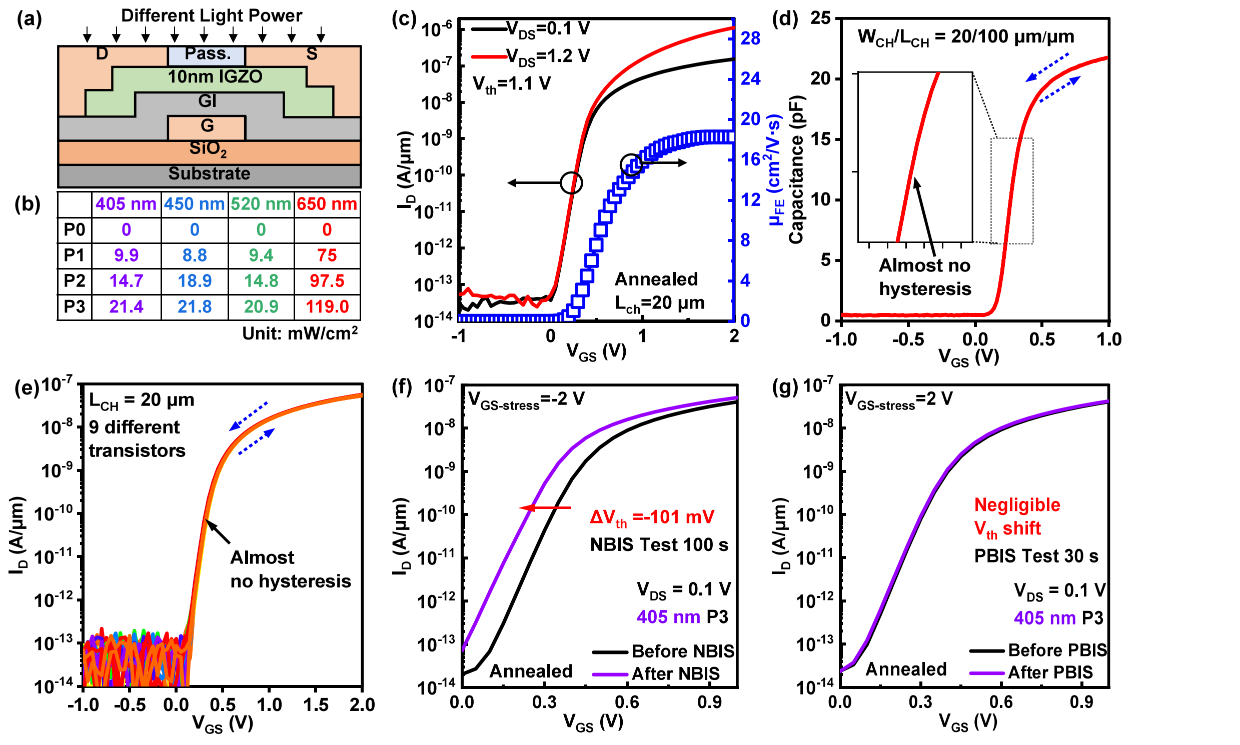

	405 nm	450 nm	520 nm	650 nm
P0	0	0	0	0
P1	9.9	8.8	9.4	75
P2	14.7	18.9	14.8	97.5
P3	21.4	21.8	20.9	119.0

Unit: mW/cm²

Figure 1. (a) Schematic diagram of an ALD IGZO transistor. The GI is 5 nm Al_2O_3 unless otherwise specified in this work. (b) Summary of light power values with different wavelengths. (c) I_D-V_{GS} and $\mu_{FE}-V_{GS}$ curves of a typical transistor after annealing. Dual-swept (d) $C-V$ and (e) $I-V$ measurements on transistors after annealing, showing almost no hysteresis and high uniformity. (f) NBIS and (g) PBIS measurements on devices with the same dimensions as those in part a. Under illumination, a negative gate bias results in a V_{th} shift, while a positive gate bias does not.

gate insulator (GI). Our results suggest that the density and impact of deep states are far less than commonly understood.

Figure 1a presents the schematic diagram of a back-gate IGZO transistor with 10 nm IGZO by ALD as the channel and 5 nm Al_2O_3 as the GI unless otherwise specified. The fabrication process of the IGZO transistors is similar to our previous work.[32] The IGZO transistors were fabricated on an 8 in. thermally oxidated p+ Si substrate. TiN was grown as a gate metal and patterned by photolithography and dry etching. GI was grown by ALD (HfO_x or AlO_x). Then, 10 nm IGZO was grown by ALD as a channel. Following channel isolation, SiO_2 was also grown by ALD as a passivation layer. After via opening, W was deposited as the source/drain metal and patterned. As-fabricated devices without annealing and devices annealed in air at 350 °C for 30 min were used as control groups. All tested devices have a channel length (L_{ch}) of 20 μm. Laser lights with different wavelengths and light powers (P) were applied, as summarized in Figure 1b. The test system adopted in this work is presented in Figure S1. Figure 1c presents the I_D-V_{GS} and $\mu_{FE}-V_{GS}$ curves of an IGZO transistor with annealing, exhibiting a field-effect mobility (μ_{FE}) of 18.3 cm^2/V·s, a threshold voltage (V_{th}) of 1.1 V, and a subthreshold swing (SS) of 67.8 mV/dec. Parts d and e of Figure 1 present the dual-swept $C-V$ and $I-V$ measurements on the transistors after annealing, showing high uniformity and negligible hysteresis. Figure 1f shows the NBIS measurement on the device with the same dimensions, showing a ΔV_{th} of −101 mV under 405 nm light illumination with a light power of 21.4 mW/mm^2 at a negative V_{GS} stress voltage ($V_{GS\text{-stress}}$) of −2 V for 100 s. Figure 1g presents a positive bias illumination stability (PBIS) measurement at V_{stress} of 2 V, exhibiting a negligible ΔV_{th} due to the high PBS performance of the IGZO transistor (Figure S2). The light stability tests suggest that positive gate bias (V_{GS} and V_{GD}) is necessary for accurate evaluation of the photocurrent (I_{ph}) in light-based methods to prevent the impact of NBIS. Figure S3 illustrates the UV–vis–near-IR (NIR) spectrum of a 15 nm IGZO thin film grown on glass, indicating that 405 nm light is sufficient for deep-state detection.

Parts a and b of Figure 2 illustrate the test waveforms in this work. For waveform 1 in Figure 2a, V_{GS} sweeps from a high voltage (V_H) to a low voltage (V_L) under dark or light illumination conditions, while V_{DS} remains at 0.1 V. For waveform 2 in Figure 2b, the light power increases after each V_{GS} sweep to evaluate the impact of carrier recombination. The first and last V_{GS} sweeps were performed under dark conditions to assess the device stability before and after illumination. The choice of V_L must not be lower than that of V_{DS} to avoid a negative gate bias. Figure 2c shows a typical measurement using waveform 1 with a V_L of −1 V. A device with a negative V_{th} was chosen to highlight the impact of NBIS. There is a permanent V_{th} shift after V_{GS} sweep under 405 nm light illumination, suggesting that an increase of the subthreshold current under illumination is the result of both photoresponse and NBIS, so that I_{ph} will be overestimated using a negative V_L. Figure 2d shows the measurements on IGZO transistors without annealing using waveform 1 with V_L of 0.1 V, where the dark I_D-V_{GS} curves before and after V_{GS} sweeps under light illumination coincide, suggesting that the NBIS effect can be ignored. To further verify that the effect of NBIS can be excluded, the measurements at a higher temperature (95 °C) were carried out and are shown in Figure S4. Therefore, avoiding a negative gate bias in light-assisted $I-V$ measurements on IGZO transistors is critical for the accurate

https://doi.org/10.1021/acs.nanolett.5c01673
Nano Lett. XXXX, XXX, XXX−XXX

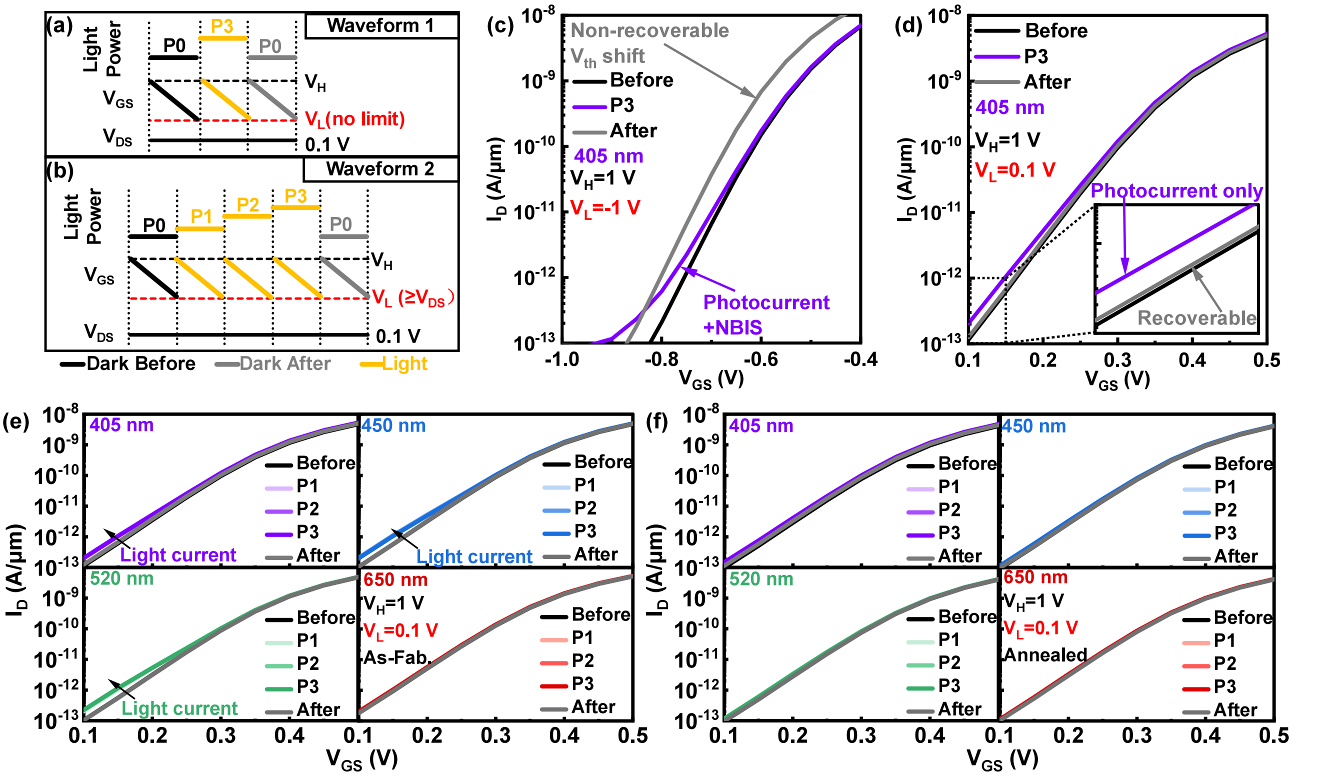

Figure 2. Test waveforms in the light-assisted $I-V$ measurements: (a) constant light power and no restriction on V_L, (b) multiple light powers and $V_L \geq V_{DS}$. V_H and V_L are the upper and lower limits of the V_{GS} sweep range, respectively. (c) Test results based on waveform 1 with a V_L of −1 V. A special device (7 nm HfO_2 as gate dielectrics and higher In content in the channel) with $V_{th} = -0.24$ V is chosen to highlight the effect of NBIS. (d) Test results based on waveform 1 with a V_L of 0.1 V. The device has the same dimensions as those in Figure 1. (e) Test results based on waveform 2 on the device without annealing under illuminations of 405, 450, 520, and 650 nm, exhibiting clear I_{ph} in the subthreshold region under 405, 450, and 520 nm illumination. (f) Test results based on waveform 2 on the device with annealing under illuminations of 405, 450, 520, and 650 nm, showing much smaller I_{ph}.

evaluation of I_{ph}, and IGZO transistors with positive V_{th} are suitable for NBIS-free light-assisted $I-V$ measurements. Figure 2e shows the measurements on IGZO transistors without annealing using waveform 2 with different wavelengths. The difference between I_D under illumination and I_D in the dark (ΔI_D) increases in the subthreshold region and is defined as the photocurrent (I_{ph}) due to electron emission from subgap defect states (including both shallow and deep states). In this work, the shallow states are defined as the defect states located near the conduction band (E_C). I_{ph} does not increase with light power from P1 to P3, indicating that most of the trapped electrons have been emitted, as will be discussed in the next part. Figure 2f shows the measurements on IGZO transistors with annealing using the same conditions as those in Figure 2e, showing less photocurrent under different illumination conditions.

The experimental I_{ph} versus P curves based on the device with and without annealing biased at $V_{GS} = 0.1$ V are shown in Figure 3a,b, where I_{ph} saturates with larger P, indicating that electrons in deep states are mostly emitted. The subgap density of states (DOS) can be calculated from light-induced I_{ph} according to $I_{ph} = n_{ph}qv$, where n_{ph} is the light-induced carrier density, q is the elementary charge, and $v = \mu E$ at low V_{DS} when the electric field (E) is low (μ is mobility). However, it is not necessary for n_{ph} to be equal to the corresponding subgap DOS because electrons in the subgap states may be partly emitted due to carrier recombination. To clarify, the emission and recombination processes under illumination are shown in Figure 3c. When the Fermi level (E_F) is low (biased at the subthreshold region), most of the shallow states are empty and the photocurrent mainly comes from electron emission from deep states. If the electrons in deep states are partly emitted, the deep-state density (N_{tD}) located between E_F and E_C-E_{ph} is much larger than the light-induced carrier density (n_{ph}). Under equilibrium conditions, the generation rate (G) and recombination rate (R) should be equal, and the equations are as follows:[33]

$$G = \frac{\sigma_n P}{h\nu}(N_{tD} - n_{ph}) \tag{1}$$

$$R = cn_{ph}N_{tA} \tag{2}$$

σ_n and c are the emission factor and the capture factor, respectively. P is the light power. N_{tA} is the density of defect states available for recombination, where N_{tA} comes from the empty shallow states above E_F and other empty states in the subgap. $h\nu$ is the photon energy. Based on eqs 1 and 2, if n_{ph} is much smaller than N_{tD}, the light power P can be derived as follows:

$$P \cong \frac{(h\nu)cN_{tA}}{\sigma_n N_{tD}}n_{ph} \propto I_{ph} \tag{3}$$

Therefore, if the deep states are partly emitted, then the photocurrent I_{ph} should be proportional to light power P. In other words, if I_{ph} is not proportional to P, we can conclude that most of the electrons in the deep states have been emitted.

https://doi.org/10.1021/acs.nanolett.5c01673
Nano Lett. XXXX, XXX, XXX−XXX

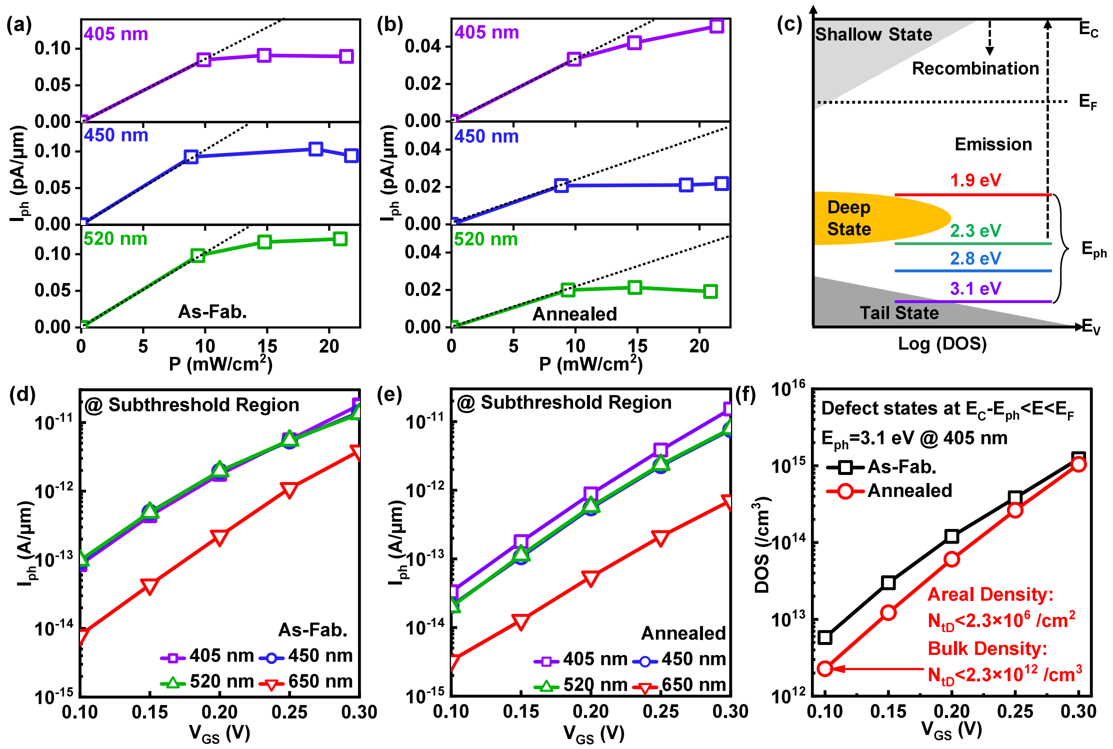

Figure 3. I_{ph} versus light power P at V_{GS} = 0.1 V of devices (a) without and (b) with annealing. The photocurrent I_{ph} is not proportional to light power P, indicating that electrons in deep states are mostly emitted. (c) Illustration of the emission and recombination process of IGZO under illumination. (d) Corresponding I_{ph} versus V_{GS} characteristics extracted from Figure 2e. (e) Corresponding I_{ph} versus V_{GS} characteristics extracted from Figure 2f. (f) DOS (all states between E_F and $E_C{-}E_{ph}$) versus V_{GS} characteristics, extracted from I_{ph} versus V_{GS} curves under 405 nm illumination, showing that N_{tD} of the annealed device is <2.3 × 10^{12}/cm^3. N_{tD} is overestimated at higher V_{GS} because of the response from shallow states below E_F.

Figure S5 presents the transient test waveform and results under 450 nm illumination on devices with and without annealing, showing that I_{ph} saturates at high P with no persistent photoconductance (PPC) effect. It can also be seen that annealing contributes to suppression of the subgap defect states.

The extracted I_{ph} versus V_{GS} characteristics of IGZO transistors without annealing are shown in Figure 3d. It can be seen that I_{ph} is much lower under 650 nm illumination but similar under 405, 450, and 520 nm illumination, inferring that electrons in shallow states are emitted by 650 nm light, while electrons in both shallow and deep states are emitted by 405, 450, and 520 nm light. In other words, deep states are mainly located at $E_C{-}E$ between 1.9 and 2.4 eV (the photon energy E_{ph} of 650 and 520 nm light). The excited electrons may come from either bulk or interface trap states. The extracted I_{ph} versus V_{GS} characteristics of IGZO transistors with annealing are shown in Figure 3e. The I_{ph} of a device with annealing reduces significantly compared to that of a device without annealing, indicating that subgap defect states are suppressed by process optimization. Note that the density of subgap defect states is related to the In−Ga−Zn component, GI material, and annealing process. Figure 3f shows the extracted DOS versus V_{GS} from I_{ph} versus V_{GS} curves under 405 nm illumination in Figure 3d,e. The extracted DOS includes part of the shallow states located below E_F and some defect states located above E_C − 1.9 eV and deep states so that the detected deep-state density is an upper limit. It was found that the detected bulk deep-state density is lower than 2.3 × 10^{12}/cm^3 (bulk density) and 2.3 × 10^6/cm^3 (areal density), which is quite a low value. Table 1 benchmarks the measured density of deep states on oxide semiconductors. The measured N_{tD} is the lowest, to the best of our knowledge, based on the NBIS-free measurements.

As is commonly understood, NBIS is related to deep states, i.e., the drifting of light-induced positive charge (due to the photoexcitation of electrons in deep states).[20] In this work, a low N_{tD} is achieved, suggesting that the ΔV_{th} caused by NBIS should be very small. However, the NBIS effect with a large ΔV_{th} still exists. The test waveform of NBIS is shown in Figure S6. Note that the $I_D{-}V_{GS}$ curves are measured under dark conditions to obtain the permanent NBIS-induced V_{th} shift, as presented in Figure S7. Figure 4a presents the NBIS measurements on an IGZO transistor with annealing under different light conditions (405, 450, and 520 nm and dark). Figure S8 summarizes the NBIS-induced ΔV_{th} versus stress time characteristics. According to Figures 4a and S8, ΔV_{th} of all transistors almost saturate after 50 s of NBIS testing, and there is a rigid shift in the $I_D{-}V_{GS}$ curves without SS degradation, suggesting that NBIS degradation is not related to the photoinduced shallow state generation, which was regarded as a possible NBIS mechanism.[21,22] Figure 4b illustrates the possible mechanism related to N_{tD}, i.e., the drifting of light-induced positive charges in deep states.[20] Figure 4c presents the NBIS-induced ΔV_{th} on an IGZO transistor with the same ALD IGZO film but different GIs (7 nm HfO_x, 7 nm AlO_x, and 5 nm AlO_x) under different light conditions. Also, the required N_{tD} (in areal density) that supports this mechanism can be estimated by $C_{ox}|\Delta V_{th}|$ and is presented in Figure 4d, where C_{ox} is the GI capacitance. The required N_{tD} is over 10^{10}/cm^2,

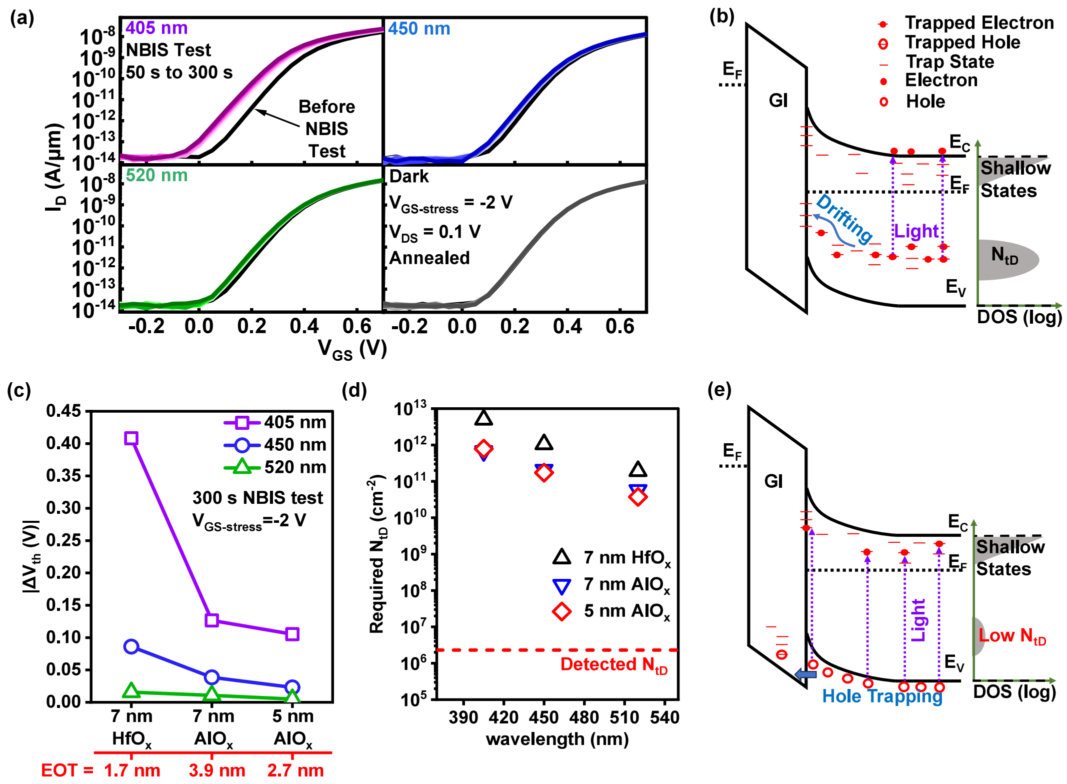

Figure 4. (a) NBIS performance of devices with annealing under different light conditions (405 nm light, 450 nm light, 520 nm light, and dark conditions). (b) Illustration of the mechanism related with deep states: the drifting of light-induced positive charges in deep states. (c) NBIS-induced ΔV_{th} of transistors with different GIs under various light conditions. (d) Required N_{tD} to support the mechanism shown in part b, indicating that the required N_{tD} is 4 orders larger than the detected N_{tD}. (e) Illustration of the light-induced hole-trapping mechanism.

which is much more than the detected value ($2.3 \times 10^6/cm^2$) in Figure 3f. Therefore, the NBIS effect is not related to the deep states in the ALD IGZO transistors. In other words, the NBIS effect for ALD IGZO transistors is not related to the mechanism of the drifting of light-induced positive charges in deep states.

As is well-known, the impact of interfacial charge (Q_f) on ΔV_{th} can be written as $\Delta V_{th} = -Q_f/C_{ox}$, where C_{ox} is the GI capacitance. Thus, the device with a larger equivalent oxide thickness (EOT), i.e., smaller C_{ox} should have a larger $|\Delta V_{th}|$ when Q_f is the same. Therefore, the drifting of light-induced positive charge (due to the photoexcitation of electrons in deep states) should contribute to a larger $|\Delta V_{th}|$ for the device with a larger EOT, which contradicts the experimental results in Figure 4c. The analysis above further confirms that this is not the main origin of the NBIS effect for ALD IGZO transistors. Because the deep-state density is low, the possible mechanism is a light-induced hole-trapping mechanism,[23] as illustrated in Figure 4e. First, electrons are excited from the valence band (E_V) to shallow states below E_C, leaving mobile holes below E_V. Second, the mobile holes are injected into the GI as hole trapping due to the negative gate bias. This mechanism is not related to deep states, and this is proven by the proposed PBS and NBIS correlation tests, as shown in Figure S9.

As can be seen, in the above NBIS-free light-assisted *I*−*V* characterization, the detected deep-state density is much lower than the previously reported values. Note that this value is still an upper limit because I_{ph} in this work is the photoresponse of both deep states and the relatively shallow states below E_F, and the photoresponse may come from both the interface and bulk traps. Therefore, it is still an open question whether there are deep-level defect states in the ALD IGZO thin film and what the corresponding defect structure of the deep state is. Even if we consider the density, we may infer that the deep-state density is so low that it may not contribute too much to the performance of ALD IGZO transistors, such as the direct-current performance, reliability, etc.

In conclusion, the ultralow N_{tD} down to $2.3 \times 10^{12}/cm^3$ in ALD IGZO transistors has been measured in this work by NBIS-free light-assisted *I*−*V* measurements, which is still an upper limit. The mechanism of NBIS is clarified according to N_{tD} measurements. The ultralow density N_{tD} suggests that deep states in ALD IGZO have a minor impact on devices with optimized processes.

■ ASSOCIATED CONTENT

Supporting Information

The Supporting Information is available free of charge at https://pubs.acs.org/doi/10.1021/acs.nanolett.5c01673.

Additional details for the photoelectrical measurement of an ALD IGZO transistor, PBS test, UV−vis−NIR spectrum, light-assisted *I*−*V* measurement at high temperature, PPC test, NBIS characterization, and PBS and NBIS correlation tests (PDF)

■ AUTHOR INFORMATION

Corresponding Authors

Ying Wu − *Huawei Technologies Company, Ltd., Shenzhen 523808, China*; Email: wuying34@hisilicon.com

Mengwei Si − *Department of Electronic Engineering and State Key Laboratory of Radio Frequency Heterogeneous Integration, Shanghai Jiao Tong University, Shanghai 200240, China;* orcid.org/0000-0003-0397-7741; Email: mengwei.si@sjtu.edu.cn

Authors

Liankai Zheng − *Department of Electronic Engineering, Shanghai Jiao Tong University, Shanghai 200240, China*
Lijuan Xing − *Huawei Technologies Company, Ltd., Shenzhen 523808, China*
Zhiyu Lin − *Department of Electronic Engineering, Shanghai Jiao Tong University, Shanghai 200240, China*
Wanpeng Zhao − *Huawei Technologies Company, Ltd., Shenzhen 523808, China*
Yuyan Fan − *Department of Nano/Microelectronics, Shanghai Jiao Tong University, Shanghai 200240, China*
Yulong Dong − *Department of Nano/Microelectronics, Shanghai Jiao Tong University, Shanghai 200240, China*
Ziheng Wang − *Department of Electronic Engineering, Shanghai Jiao Tong University, Shanghai 200240, China*
Siying Li − *Department of Electronic Engineering and State Key Laboratory of Radio Frequency Heterogeneous Integration, Shanghai Jiao Tong University, Shanghai 200240, China*
Xiuyan Li − *Department of Nano/Microelectronics, Shanghai Jiao Tong University, Shanghai 200240, China*
Jeffrey Xu − *Huawei Technologies Company, Ltd., Shenzhen 523808, China*

Complete contact information is available at:
https://pubs.acs.org/10.1021/acs.nanolett.5c01673

Author Contributions

L.Z. conceived the idea for a NBIS-free light-assisted $I-V$ method. L.X. and W.Z. fabricated IGZO transistors for testing. L.Z., L.X., Z.L., Y.F., and Y.D. performed the NBIS-free light-assisted $I-V$ measurements and NBIS characterization. L.Z., L.X., Z.W., S.L., X.L., Y.W., J.X., and M.S. conducted all data analysis. L.Z. and M.S. cowrote the manuscript, and all authors commented on it.

Notes

The authors declare no competing financial interest.

■ ACKNOWLEDGMENTS

This work was supported by the National Natural Science Foundation of China (Nos. 92264204, 62274107, and 62104143) and Shanghai Pilot Program for Basic Research-Shanghai Jiao Tong University under Grant 21TQ1400212.

■ REFERENCES

(1) Nomura, K.; Ohta, H.; Takagi, A.; Kamiya, T.; Hirano, M.; Hosono, H. Room-Temperature Fabrication of Transparent Flexible Thin-Film Transistors Using Amorphous Oxide Semiconductors. *Nature* **2004**, *432* (7016), 488−492.

(2) Lee, S.; Nathan, A.; Robertson, J.; Ghaffarzadeh, K.; Pepper, M.; Jeon, S.; Kim, C.; Song, I.-H.; Chung, U.-I.; Kim, K. Temperature Dependent Electron Transport in Amorphous Oxide Semiconductor Thin Film Transistors. *IEEE International Electron Devices Meeting*; IEEE, 2011; pp 343−346.

(3) Jeon, S.; Ahn, S.-E.; Song, I.; Kim, C. J.; Chung, U.-I.; Lee, E.; Yoo, I.; Nathan, A.; Lee, S.; Ghaffarzadeh, K.; Robertson, J.; Kim, K. Gated Three-Terminal Device Architecture to Eliminate Persistent Photoconductivity in Oxide Semiconductor Photosensor Arrays. *Nat. Mater.* **2012**, *11* (4), 301−305.

(4) Lee, S.; Nathan, A. Subthreshold Schottky-Barrier Thin-Film Transistors with Ultralow Power and High Intrinsic Gain. *Science* **2016**, *354* (6310), 302−306.

(5) Hosono, H. How We Made the IGZO Transistor. *Nat. Electron.* **2018**, *1* (7), 428−429.

(6) Ide, K.; Nomura, K.; Hosono, H.; Kamiya, T. Electronic Defects in Amorphous Oxide Semiconductors: A Review. *Phys. Status Solidi A* **2019**, *216* (5), No. 1800372.

(7) Li, S.; Tian, M.; Gao, Q.; Wang, M.; Li, T.; Hu, Q.; Li, X.; Wu, Y. Nanometre-Thin Indium Tin Oxide for Advanced High-Performance Electronics. *Nat. Mater.* **2019**, *18* (10), 1091−1096.

(8) Chakraborty, W.; Grisafe, B.; Ye, H.; Lightcap, I.; Ni, K.; Datta, S. BEOL Compatible Dual-Gate Ultrathin-Body W-Doped Indium-Oxide Transistor with I_{on} = 370 μA/μm, SS = 73 mV/dec and I_{on}/I_{off} Ratio > 4 × 10^9. *Proceedings of the IEEE Symposium on VLSI Technology*; IEEE, 2020; pp TH2.1.1−TH2.1.2.

(9) Belmonte, A.; Oh, H.; Subhechha, S.; Rassoul, N.; Hody, H.; Dekkers, H.; Delhougne, R.; Ricotti, L.; Banerjee, K.; Chasin, A.; van Setten, M. J.; Puliyalil, H.; Pak, M.; Teugels, L.; Tsvetanova, D.; Vandersmissen, K.; Kundu, S.; Heijlen, J.; Batuk, D.; Geypen, J.; Goux, L.; Kar, G. S. Tailoring IGZO-TFT Architecture for Capacitorless DRAM, Demonstrating >10^3 s Retention, >10^{11} Cycles Endurance and L_g Scalability Down to 14 nm. *IEEE International Electron Devices Meeting*; IEEE, 2021; pp 226−229.

(10) Wu, J.; Mo, F.; Saraya, T.; Hiramoto, T.; Ochi, M.; Goto, H.; Kobayashi, M. Mobility-Enhanced FET and Wakeup-Free Ferroelectric Capacitor Enabled by Sn-doped InGaZnO for 3D Embedded RAM Application. *Proceedings of the IEEE Symposium on VLSI Technology*; IEEE, 2021; pp T6-2.1−T6-2.2.

(11) Duan, X.; Huang, K.; Feng, J.; Niu, J.; Qin, H.; Yin, S.; Jiao, G.; Leonelli, D.; Zhao, X.; Jing, W.; Wang, Z.; Chen, Q.; Chuai, X.; Lu, C.; Wang, W.; Yang, G.; Geng, D.; Li, L.; Liu, M. Novel Vertical Channel-All-Around (CAA) IGZO FETs for 2T0C DRAM with High Density beyond $4F^2$ by Monolithic Stacking. *IEEE International Electron Devices Meeting*; IEEE, 2021; pp 222−225.

(12) Si, M.; Lin, Z.; Chen, Z.; Sun, X.; Wang, H.; Ye, P. D. Scaled Indium Oxide Transistors Fabricated Using Atomic Layer Deposition. *Nat. Electron.* **2022**, *5* (3), 164−170.

(13) Wang, C.; Kumar, A.; Han, K.; Sun, C.; Xu, H.; Zhang, J.; Kang, Y.; Kong, Q.; Zheng, Z.; Wang, Y.; Gong, X. Extremely Scaled Bottom Gate a-IGZO Transistors Using a Novel Patterning Technique Achieving Record High G_m of 479.5 μS/μm (V_{DS} of 1 V) and fT of 18.3 GHz (V_{DS} of 3 V). *Proceedings of the IEEE Symposium on VLSI Technology*; IEEE, 2022; pp 294295

(14) Liu, G.; Kong, Q.; Wang, X.; Tu, Y.-H.; Zheng, Z.; Sun, C.; Zhang, D.; Kang, Y.; Han, K.; Liang, G.; Gong, X. Unveiling the Influence of Channel Thickness on PBTI and LFN in Sub-10 nm-Thick IGZO FETs: A Holistic Perspective for Advancing Oxide Semiconductor Devices. *IEEE International Electron Devices Meeting*; IEEE, 2023; pp 41.4.1−41.4.4.

(15) Liu, G.; Kong, Q.; Zhou, Z.; Xu, Y.; Sun, C.; Han, K.; Kang, Y.; Zhang, D.; Wang, X.; Feng, Y.; Shi, W.; Nguyen, B.-Y.; Ni, K.; Liang, G.; Gong, X. Unveiling the Impact of AC PBTI on Hydrogen Formation in Oxide Semiconductor Transistors. *Proceedings of the IEEE Symposium on VLSI Technology*; IEEE, 2024; pp T16.1.1−T16.1.2.

(16) Deng, S.; Kwak, J.; Lee, J.; Chakraborty, D.; Shin, J.; Phadke, O.; Kirtania, S. G.; Zhang, C.; Aabrar, K. A.; Yu, S.; Datta, S. Demonstration of On-Chip Switched-Capacitor DC−DC Converters using BEOL Compatible Oxide Power Transistors and Superlattice MIM Capacitors. *Proceedings of the IEEE Symposium on VLSI Technology*; IEEE, 2024; pp TFS1.3.1−TFS1.3.2.

(17) Liu, M.; Li, Z.; Lu, W.; Chen, K.; Niu, J.; Liao, F.; Wu, Z.; Lu, C.; Li, W.; Geng, D.; Lu, N.; Dou, C.; Yang, G.; Li, L.; Liu, M. First Demonstration of Monolithic Three-Dimensional Integration of Ultra-High-Density Hybrid IGZO/Si SRAM and IGZO 2T0C DRAM Achieving Record-Low Latency (<10 ns), Record-Low Energy (<10 fJ) of Data Transfer and Ultra-Long Data Retention

(>5000 s). *Proceedings of the IEEE Symposium on VLSI Technology*; IEEE, 2024; pp T12.3.1−T12.3.2.

(18) Nomura, K.; Kamiya, T.; Yanagi, H.; Ikenaga, E.; Yang, K.; Kobayashi, K.; Hirano, M.; Hosono, H. Subgap States in Transparent Amorphous Oxide Semiconductor, In-Ga-Zn-O, Observed by Bulk Sensitive X-ray Photoelectron Spectroscopy. *Appl. Phys. Lett.* **2008**, *92* (20), No. 202117.

(19) Bang, J.; Matsuishi, S.; Hosono, H. Hydrogen Anion and Subgap States in Amorphous In-Ga-Zn-O Thin Films for TFT Applications. *Appl. Phys. Lett.* **2017**, *110* (23), No. 232105.

(20) Nomura, K.; Kamiya, T.; Hosono, H. Highly Stable Amorphous In-Ga-Zn-O Thin-film Transistors Produced by Eliminating Deep Subgap Defects. *Appl. Phys. Lett.* **2011**, *99* (5), No. 053505.

(21) Lee, M.; Kim, M.; Jo, J.-W.; Park, S. K.; Kim, Y.-H. Suppression of Persistent Photo-Conductance in Solution-Processed Amorphous Oxide Thin-Film Transistors. *Appl. Phys. Lett.* **2018**, *112* (5), No. 052103.

(22) Chen, C.-K.; Xu, Z.; Hooda, S.; Pan, J.; Zamburg, E.; Thean, A. V.-Y. Negative-U Defect Passivation in Oxide-Semiconductor by Channel Defect Self-Compensation Effect to Achieve Low Bias Stress V_{TH} Instability of Low-Thermal Budget IGZO TFT and FeFETs. *IEEE International Electron Devices Meeting*; IEEE, 2023; pp 41.2.1−41.2.4.

(23) Kim, H.; Im, K.; Park, J.; Khim, T.; Hwang, H.; Kim, S.; Lee, S.; Song, M.; Choi, P.; Song, J.; Choi, B. The Effects of Valence Band Offset on Threshold Voltage Shift in a-InGaZnO TFTs Under Negative Bias Illumination Stress. *IEEE Electron Device Lett.* **2020**, *41* (5), 737−740.

(24) Mattson, G. W.; Vogt, K. T.; Wager, J. F.; Graham, M. W. Hydrogen Incorporation into Amorphous Indium Gallium Zinc Oxide Thin-film Transistors. *J. Appl. Phys.* **2022**, *131* (10), No. 105701.

(25) Wu, Z.; Chasin, A.; Franco, J.; Subhechha, S.; Dekkers, H.; Bhuvaneshwari, Y. V.; Belmonte, A.; Rassoul, N.; van Setten, M. J.; Afanas'ev, V.; Delhougne, R.; Kaczer, B.; Kar, G. S. Characterizing and Modelling of the BTI Reliability in IGZO-TFT using Light-Assisted I-V Spectroscopy. *IEEE International Electron Devices Meeting*; IEEE, 2022; pp 695−698.

(26) Bae, H.; Seo, H.; Jun, S.; Choi, H.; Ahn, J.; Hwang, J.; Lee, J.; Oh, S.; Bae, J.-U.; Choi, S.-J.; Kim, D. H.; Kim, D. M. Fully Current-Based Sub-Bandgap Optoelectronic Differential Ideality Factor Technique and Extraction of Subgap DOS in Amorphous Semiconductor TFTs. *IEEE Trans. Electron Devices* **2014**, *61* (10), 3566−3572.

(27) Mattson, G. W.; Vogt, K. T.; Wager, J. F.; Graham, M. W. Illuminating Trap Density Trends in Amorphous Oxide Semiconductors with Ultrabroadband Photoconduction. *Adv. Funct. Mater.* **2023**, *33* (25), No. 2300742.

(28) Bae, H.; Choi, H.; Jun, S.; Jo, C.; Kim, Y. H.; Hwang, J. S.; Ahn, J.; Oh, S.; Bae, J.-U.; Choi, S.-J.; Kim, D. H.; Kim, D. M. Single-Scan Monochromatic Photonic Capacitance-Voltage Technique for Extraction of Subgap DOS over the Bandgap in Amorphous Semiconductor TFTs. *IEEE Electron Device Lett.* **2013**, *34* (12), 1524−1526.

(29) Choi, S.; Kim, J.-Y.; Rhee, J.; Kang, H.; Park, S.; Kim, D. M.; Choi, S.-J.; Kim, D. H. Method to Extract Interface and Bulk Trap Separately over the Full Sub-Gap Range in Amorphous InGaZnO Thin-Film Transistors by Using Various Channel Thicknesses. *IEEE Electron Device Lett.* **2019**, *40* (4), 574−577.

(30) Yang, G. W.; Park, J.; Choi, S.; Kim, C.; Kim, D. M.; Choi, S.-J.; Bae, J.-H.; Cho, I. H.; Kim, D. H. Total Subgap Range Density of States-Based Analysis of the Effect of Oxygen Flow Rate on the Bias Stress Instabilities in a-IGZO TFTs. *IEEE Trans. Electron Devices* **2022**, *69* (1), 166−172.

(31) Rinaudo, P.; Chasin, A.; Zhao, Y.; Kaczer, B.; Rassoul, N.; Dekkers, H. F. W.; Setten, M. J.; Belmonte, A.; Wolf, I. D.; Kar, G. S.; Franco, J. Light-Assisted Investigation of the Role of Oxygen Flow during IGZO Deposition on Deep Subgap States and Their Evolution under PBTI. *IEEE International Reliability Physics Symposium*; IEEE, 2024; pp 5A.3.1−5A.3.9.

(32) Lin, Z.; Kang, L.; Zhao, J.; Yin, Y.; Wang, Z.; Yu, J.; Li, Y.; Yi, G.; Nathan, A.; Li, X.; Wu, Y.; Xu, J.; Si, M. The Role of Oxygen Vacancy and Hydrogen on the PBTI Reliability of ALD IGZO Transistors and Process Optimization. *IEEE Trans. Electron Devices* **2024**, *71* (5), 3002−3008.

(33) Schroder, D. K. *Semiconductor Material and Device Characterization*, 3rd ed.; Wiley: Hoboken, NJ, 2006.

https://doi.org/10.1021/acs.nanolett.5c01673
Nano Lett. XXXX, XXX, XXX−XXX